Geochemical Perspectives Letters

The rises and falls of zirconium isotopes during zircon crystallisation

I.N. Bindeman[1*], O.E. Melnik[2]

https://doi.org/10.7185/geochemlet.2241

Abstract

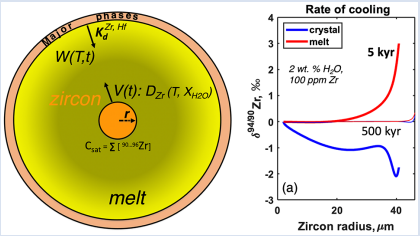

Zircon trace element and isotopic analysis for an increasing number of isotopic systems provide valuable insights into magma crystallisation, and evolution of the continental crust. Zirconium stable isotopes have been measured recently and shown to vary by several per mille on Earth. Both positive and negative shifts of $\delta^{94/90}$Zr have been found in zircons and melts, and equilibrium isotopic fractionations are found to be small. We here employ and further develop a zircon crystallisation programme with two moving boundaries targeting zircon crystallisation in the presence of other minerals. We reproduce positive, negative, and inverse $\delta^{94/90}$Zr, Zr/Hf, and other compatible trace element variations in zircon and surrounding melt that can be entirely explained by the boundary layer processes during kinetics of zircon crystallisation in a realistic set of geologic conditions. Progressively lower $\delta^{94/90}$Zr values in zircon develop during rapid crystallisation, lower melt water contents, crystallisation in the lower temperature range, and whilst co-crystallising with the Zr-poor phase. Given large (multi-per mille) kinetic Zr isotope fractionations discovered, zircon may serve as a monitor of magmatic crystallisation conditions, but is unlikely to serve as a diagnostic tool for the bigger set of petrological problems (*e.g.*, evolution of the continental crust) without proper context.

Received 15 September 2022 | Accepted 21 November 2022 | Published 9 December 2022

Letter

There is an unprecedented increase in use of non-traditional stable isotopes fuelled by analytical advances in geochemistry and cosmochemistry (Watkins *et al.*, 2017). After a certain system becomes analytically possible, development proceeds in the following sequence: 1) to find measurable ranges of variations, 2) to interpret their origin, 3) to find exciting applications that solve urgent geological problems (Aarons *et al.*, 2021), 4) to critically appraise the new results, and finally 5) "settling" the new isotopic system as "conventional" with well-established measurement protocols and range of uses. Zircon is a unique mineral that is being used extensively for U-Th-Pb geochronology, trace element variations, O, Li and radiogenic Hf variations, and as such it has seen many of these "rises" and "falls". As we demonstrate below, this may characterise their Zr isotope variations, a subject of much recent research.

Zirconium has five stable isotopes and the 94/90 ratio expressed as $\delta^{94/90}$Zr relative to a standard is commonly used to understand its variations (Inglis *et al.*, 2018, 2019). This ratio can be measured with good sub-per mille precision in rocks, major minerals, and *in situ* inside zircons by either SIMS or LA-ICP-MS methods, permitting core to rim, or face to core profiles (Ibañez-Mejia and Tissot, 2019; Zhang *et al.*, 2019; Guo *et al.*, 2020; Tompkins *et al.*, 2020). Inglis *et al.* (2019) demonstrated a 0.5 ‰ positive shift in a single silicic magmatic suite of Hekla volcano (Iceland), which the authors interpreted as the result of igneous fractionations of isotopically light zircons. At the same time, Ibañez-Mejia and Tissot (2019) studied zircons in the Duluth gabbro and found most of them isotopically heavier than the melt from which they crystallised (thus discovering an opposite trend of Zr isotopic fractionation), yet they also found a few extremely low $\delta^{94/90}$Zr grains, with the range covering almost 5 ‰. Guo *et al.* (2020) measured $\delta^{94/90}$Zr in individual zircon grains and found lighter cores and heavier rims, while Tompkins *et al.* (2020) found no isotopic differences in a large zircon megacryst that crystallised from carbonatitic magma. Given the large $\delta^{94/90}$Zr ranges of several per mille discovered, Tian *et al.* (2021) suggested that Zr isotopes can be used to monitor continental crust evolution since the Archean, and also to provide a new tool to investigate the origin of the earliest crust. The field is rapidly developing and thus requires better understanding of what controls Zr isotopic variations in nature. This question has been recently addressed by Chen *et al.* (2020), Méheut *et al.* (2021), and Tissot and Ibañez-Mejia (2021), among others. Theoretical *ab initio* modelling (Méheut *et al.*, 2021) returns very small <0.1 ‰ equilibrium melt-zircon fractionations at realistic high temperature (>600 °C) conditions, when zircon is able to crystallise from magma, down to the low temperature of water saturated pegmatites. These authors, Tissot and Ibañez-Mejia (2021) and Aarons *et al.* (2021) suggested that kinetic effects likely dominate the Zr isotope variations in nature, *via* faster diffusion of light isotopes of zirconium during zircon crystallisation from magmas, and in front of crystallising major minerals.

We here present the result of numerical modelling of Zr isotopes and Zr/Hf ratios during zircon crystallisation, based

1. Department of Earth Sciences, University of Oregon, Eugene, OR, USA
2. Institute of Mechanics, Lomonosov Moscow State University, Moscow, Russia
* Corresponding author (email: bindeman@uoregon.edu)

on the further development of the Bindeman and Melnik (2016) and Melnik and Bindeman (2018) models. In short, the model is realised in spherical coordinates, in which zircon is growing from the centre and other minerals are forming on the outer cell boundary (Fig. 1) by following a *T*-*X* (% crystals) phase diagram. Upon cooling and solidification, zircon grows outward and other minerals advance inward, decreasing the proportion of melt in the cell. The melt compositional parameter, M factor (Harrison and Watson, 1983), that determines zircon solubility is taken into account *via* its temperature-compositional dependence as in Bindeman and Melnik (2016). Zirconium, its isotopes, and other trace element diffusion coefficients are parameterised as a function of temperature and water content based on Zhang *et al.* (2010). Since each zirconium isotope has a large abundance, for this work we have rewritten saturation boundary conditions at the zircon/melt boundary, so they add together to total [Zr] at C_{sat} at each *T* and M factor (Fig. 1). Mass conservation in the entire melt cell is obeyed (Fig. S-1).

We assume that different isotopes of zirconium diffuse with different rates in proportion to their mass, following a mass dependent relationship of diffusion coefficients *via* a kinetic law with a beta exponent parameter $\beta = 0.05$ (Watkins *et al.*, 2017). Variations in this parameter within a reasonable ±0.02 range are less important than isotopic effects unravelled due to, for example, cooling rates and other crystallisation conditions described below. The outer boundary on which major minerals crystallise has a condition of Zr (and Hf) partitioning in accordance with their Zr partition coefficient, K_d, set by the user. As Zr and Hf are highly incompatible in most minerals, K_d is <<1; however, we also experimented by making this K_d around 1 for the case of amphibole, ±micro-zircon or sphene inclusion co-precipitation. We also implemented and monitored the behaviour of U, Th, Y, P, and Ti (Fig. S-4).

We performed a series of computations (Figs. 2, 3 and S-3 to S-5) of zircon crystallisation from magma during linear cooling from 900 to 650 °C by varying 1) zircon crystallisation duration increasing from 150 years to 0.5 Myr, 2) zircon crystallisation in low and high temperature ranges, achievable by increasing and decreasing Zr concentrations in the initial melt, 3) co-crystallisation of minerals with different Zr partition coefficients, and 4) crystallisation of magmas with different water contents. These parameters capture most of the conditions in nature. Figure 2 presents diffusion profiles through the melt cell initially containing 100 ppm Zr, showing Zr isotopic and Zr/Hf distribution in a typical run at realistic geologic parameters. Notice evolving sigmoidal shapes explained by the crystallisation of zircon and major minerals. We additionally consider Hf concentration and monitor Zr/Hf ratio. Hf is an element twin for zirconium with an identical ionic radius, 4+ charge, and thus extremely close chemical properties (partitioning with $K_d \approx 10^3$–10^4). However, because of its greater mass (174–180), Hf is expected to diffuse more slowly in melts, similar to the heaviest Zr isotope.

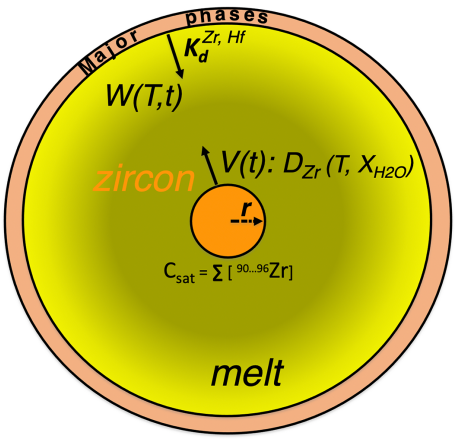

Figure 1 Zircon crystallisation from melt in a cell with two moving boundaries (*V*, *W*) employed in this model. Isotopes of zirconium move through the melt with diffusion coefficients in accordance with the mass dependence law, $D_x/D_{90} = (x/90)^{\beta}$, where β is taken as 0.05 (Watkins *et al.*, 2017; Méheut *et al.*, 2021). The proportion of melt changes in accordance with a phase diagram as a function of temperature. The zircon/melt saturation condition is a sum of all isotopes that add up to bulk C_{sat} for Zr. The outer boundary of the melt cell (with crystallising major minerals) does not discriminate against isotopes of Zr. Partition and diffusion coefficients are temperature dependent and D_{Zr} is also [H_2O] dependent.

The main result of this study is that we observe positive, negative, and inverse $\delta^{94/90}$Zr values and Zr/Hf ratios (Figs. 3, 4). Notice that this diversity of isotopic results can explain the range, as well as both positive and negative $\delta^{94/90}$Zr values observed in nature. Furthermore, a simultaneous change of these parameters and more complicated cooling and heating paths can lead to further complexity of Zr isotope behaviour, which can enhance or diminish gradual trends in Figure 3. Some general statements can also be made. Given the faster diffusion of ^{90}Zr, zircon is predicted to decrease in $\delta^{94/90}$Zr from core to rim upon its sole growth in a cell. These effects are very small (<0.1 ‰) to almost non-existent at high *T*, high H_2O and large melt cells when diffusion coefficients for both ^{90}Zr and ^{94}Zr are high, leading to lack of any $\delta^{94/90}$Zr zoning. Melt cells around zircons evolve toward higher $\delta^{94/90}$Zr values (Fig. 2). Crystallisation of the other minerals on the outer boundary (set here not to discriminate Zr isotopes) leads to piling up (bulldozing) effects and higher $\delta^{94/90}$Zr values and Zr/Hf ratios due to effects of zircon crystallisation on the inside. It is thus expected that major minerals too, will have diversity of $\delta^{94/90}$Zr and Zr/Hf ratios due to zircon co-crystallisation despite having overall low Zr and Hf concentrations. Therefore, simultaneous crystallisation of zircon and major minerals leads to a complex $\delta^{94/90}$Zr distance profile (Fig. 2) and diverse $\delta^{94/90}$Zr isotopic trends (Fig. 2).

In nature, after zircon saturation, both Zr and Hf decrease in melts, but Hf is decreasing less, and thus the Zr/Hf ratio in rocks decreases by a factor of 2–3 from basalt to rhyolites with the progress of igneous differentiation (Claiborne *et al.*, 2006). Figure 4 plots the Zr/Hf ratio in zircons at different conditions and shows them to be a strong function of crystallisation parameters. During a long duration of crystallisation, in melts with greater water concentrations, Zr and Hf diffusion toward zircon's growing boundary are near equilibrium, generating nearly identical Zr/Hf profiles within a zircon. If the crystallisation of zircon is rapid, from water-poor melt, with slow overall diffusion, and fast growth rates, then differences in Zr and Hf diffusion coefficients create kinetic disequilibrium conditions, and the zircon develops positive, negative, and inverse Zr/Hf profiles, with secondary kinks at the end of crystallisation and toward the zircon rim explained by co-crystallisation of Zr-and Hf-poor phases on the outside of the cell (Fig. 1).

Overall, the Zr/Hf chemical ratio follows the $\delta^{94/90}$Zr trends (compare Fig. 4 to Fig. 3), positive at fast crystallisation and negative at slow. Both $\delta^{94/90}$Zr and Zr/Hf ratios in growing zircons become lower for greater zircon growth rates, where the diffusive boundary layer around zircon favours light isotopes and Zr over Hf. Again, this is realised with greater rates of cooling, lower water, larger cells, and lower Zr concentrations. In our previous model targeting element partitioning into zircon, Hf concentration decreases toward the rim as a strong function of the rate of cooling (see Fig. 7 in Melnik and Bindeman, 2018),

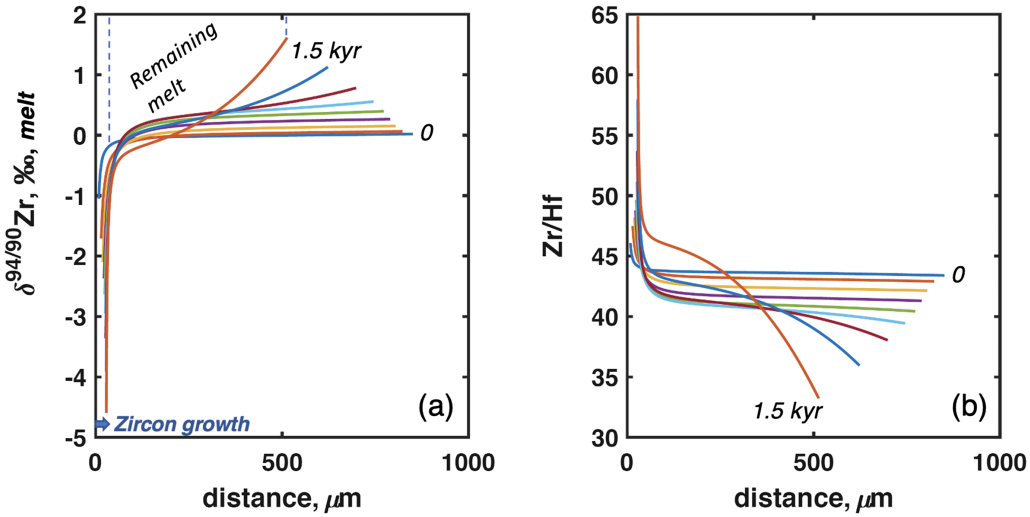

Figure 2 δ^{94}Zr and Zr/Hf profiles through the crystallising melt cell over 1.5 kyr. See Figure S-3 for profiles during longer crystallisation durations.

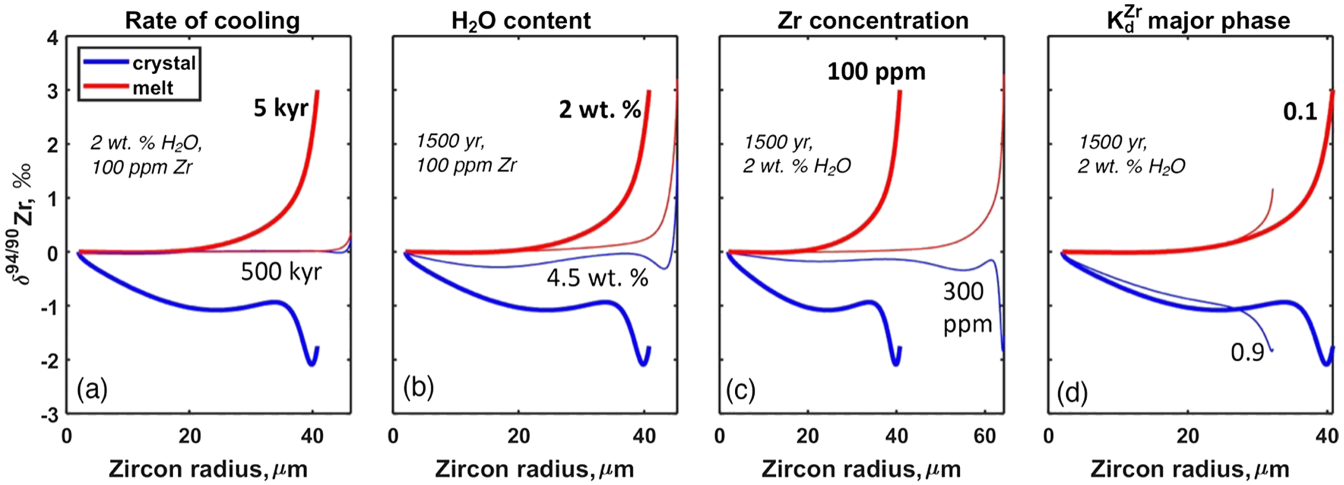

Figure 3 Variation of Zr isotopic ratios in a growing zircon crystal (blue) and surrounding melt, averaged over the remaining melt volume in the cell for each corresponding zircon radius (red), as a function of **(a)** rate of cooling, **(b)** water content in melt, **(c)** Zr concentration (*T* of saturation), and **(d)** K_d of Zr in the major phase on the outer boundary of the cell (Fig. 1). Crystallisation proceeds to 0.5 mm melt radius in an initial 1 mm cell during linear cooling; zircon reaches different final radii depending on the crystallisation parameters. Isotopic inversions seen on graphs are related to the effects of a major mineral crystallisation that lead to the piling up of Zr. Crystallisation of major minerals is set so as not to discriminate between Zr isotopes in the current model.

matching natural observations (Claiborne *et al.*, 2006, 2018). It is expected that Hf stable isotopes (^{176}Hf/^{177}Hf ratio) will behave in a similar manner to ^{94}Zr/^{90}Zr isotopes during zircon crystallisation; Hf is a highly compatible element in zircon ($K_d > 1000$) and thus isotopic preferences for isotopically light ^{176}Hf are set at the zircon-melt interface in the same way as for Zr isotopes. Computed affects (Fig. S-5) are smaller than 1 ‰, but because Hf isotopes are measured in ε(^{176}Hf/^{177}Hf) units (which are 10× the δ scale), these are not negligible in affecting primary radiogenic Hf ratios. Supplementary Figure S-4 plots other trace element ratios that are easy to compute within the present model. The behaviour of highly compatible elements in zircon (U, Th, Y, P) is comparable to that of Hf (with piling up and inversions at fast crystallisation) with some nuances related to their diffusion coefficients and K_d.

Incompatible trace elements, such as Ti behave much more simply without inversions. Considering isotopes of other incompatible trace elements that partition in zircons, *e.g.*, ^{143}Nd/^{144}Nd and ^{7}Li/^{6}Li, requires further development of the present model, but since these are incompatible, no kinetic isotope effects are expected due to zircon growth. Crystallisation of major minerals with different K_d on the outer cell boundary may further influence zircon growth and its element behaviour, however, due to the small size of zircon and the cubic relation of melt cell volume *vs.* its remaining radius, only very advanced degrees of crystallisation (>90 %) would produce piling up effects reflected in zircons.

The main result of the present work is a strong dependency of $\delta^{94/90}$Zr and Zr/Hf ratios on crystallisation parameters. The software that we offer as a part of this paper (https://github.com/crystalworkshop/isotop_diffusion) can be used by practitioners to interrogate their specific situations of magmatic cooling and zircon growth, including other trace elements (Fig. S-4). As $\delta^{94/90}$Zr will soon become an easy to obtain parameter in zircon research for a wide number of users (similar to how Ti in zircon, for example, is now used), the present approach will help to understand variations in both $\delta^{94/90}$Zr and Zr/Hf ratios.

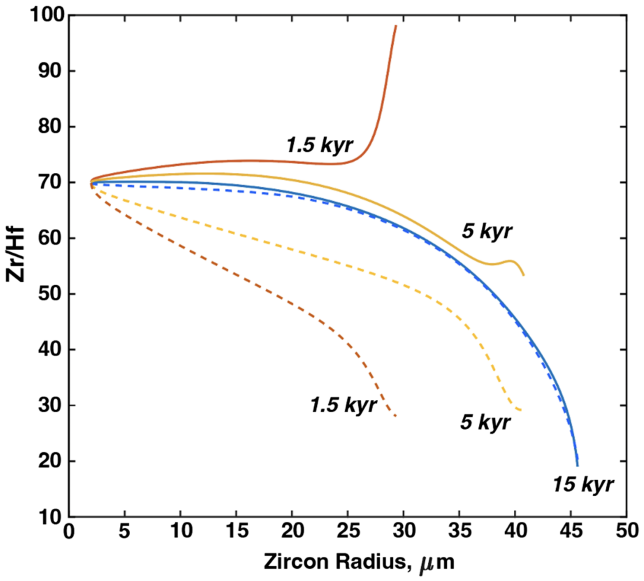

Figure 4 Zr/Hf ratio within crystallising zircons as a function of duration of crystallisation and assumed diffusion coefficient ratios in the melt ($D_{Hf}/D_{Zr} = 0.5$, solid lines; 1.5, dashed lines). Note that zircons grow bigger with longer crystallisation duration. See Figure S-4 for other trace elements and Figure S-5 for $^{176}Hf/^{177}Hf$ behaviour.

Specific conditions of magmatic crystallisation, as well as the presence or absence of Rayleigh fractionation, in which an incrementally different $\delta^{94/90}Zr$ zircon or melt are removed or added to the system (such as in the classic example of Hekla) will explore the wealth of natural situations. A few general statements as a result of the modelling can be mentioned: higher temperature of crystallisation, slower rates and a longer duration of zircon growth, higher water contents of magma, and higher $K_d(Zr)$ of co-crystallising phase all lead to minimal isotopic differences; the opposite processes lead to initially more negative $\delta^{94/90}Zr$, which then invert with values spanning several per mille.

The present model provides an easy test for two prevailing end member models of silicic magma petrogenesis: 1) slow crystallisation with melt segregation in large mushy reservoirs *vs.* 2) rapid crystallisation in individual dike and sills, accreting during batholith/magma chamber construction, followed by storage with limited zircon core recrystallisation. The first scenario should result in no core to rim $\delta^{94/90}Zr$ zoning, while the second case should result in significant $\delta^{94/90}Zr$ core to rim variations (and Zr/Hf, plus other trace elements zoning). Trace element concentrations and ratios (*e.g.*, Figs. 4, S-4) should also reflect these processes, and our model provides a platform for investigating their behaviours in zircons from different magmatic regimes and throughout geologic history.

Data and Materials Availability

The MATLAB Code and User Guide are available from GitHub: https://github.com/crystalworkshop/isotop_diffusion.

Acknowledgements

We thank Francois Tissot and Mauricio Ibañez-Mejia for constructive reviews and Helen Williams for editorial comments. Supported by NSF Grant EAR1833420.

Editor: Helen Williams

Additional Information

Supplementary Information accompanies this letter at https://www.geochemicalperspectivesletters.org/article2241.

Cite this letter as: Bindeman, I.N., Melnik, O.E. (2022) The rises and falls of zirconium isotopes during zircon crystallisation. *Geochem. Persp. Let.* 24, 17–21. https://doi.org/10.7185/geochemlet.2241

References

Aarons, S.M., Johnson, A.C., Rader, S.T. (2021) Forming Earth's Continental Crust: A Nontraditional Stable Isotope Perspective. *Elements* 17, 413–418. https://doi.org/10.2138/gselements.17.6.413

Bindeman, I.N., Melnik, O.E. (2016) Zircon Survival, Rebirth and Recycling during Crustal Melting, Magma Crystallization, and Mixing Based on Numerical Modelling. *Journal of Petrology* 57, 437–460. https://doi.org/10.1093/petrology/egw013

Chen, X., Wang, W., Zhang, Z., Nie, N.X., Dauphas, N. (2020) Evidence from *Ab Initio* and Transport Modeling for Diffusion-Driven Zirconium Isotopic Fractionation in Igneous Rocks. *ACS Earth and Space Chemistry* 4, 1572–1595. https://doi.org/10.1021/acsearthspacechem.0c00146

Claiborne, L.L., Miller, C.F., Walker, B.A., Wooden, J.L., Mazdab, F.K., Bea, F. (2006) Tracking magmatic processes through Zr/Hf ratios in rocks and Hf and Ti zoning in zircons: An example from the Spirit Mountain batholith, Nevada. *Mineralogical Magazine* 70, 517–543. https://doi.org/10.1180/0026461067050348

Claiborne, L.L., Miller, C.F., Gualda, G.A.R., Carley, T.L., Covey, A.K., Wooden, J.L., Fleming, M.A. (2018) Zircon as Magma Monitor: Robust, Temperature-Dependent Partition Coefficients from Glass and Zircon Surface and Rim Measurements from Natural Systems. In: Moser, D.E., Corfu, F., Darling, J.R, Reddy, S.M., Tait, K. (Eds.) *Microstructural Geochronology: Planetary Records Down to Atom Scale. Geophysical Monograph 232*, American Geophysical Union, Washington, D.C., John Wiley and Sons, Inc., Hoboken, NJ, 1–33. https://doi.org/10.1002/9781119227250.ch1

Guo, J.-L., Wang, Z., Zhang, W., Moynier, F., Cui, D., Hu, Z., Ducea, M.N. (2020) Significant Zr isotope variations in single zircon grains recording magma evolution history. *Proceedings of the National Academy of Sciences* 117, 21125–21131. https://doi.org/10.1073/pnas.2002053117

Ibañez-Mejia, M., Tissot, F.L.H. (2019) Extreme Zr stable isotope fractionation during magmatic fractional crystallisation. *Science Advances* 5, eaax8648. https://doi.org/10.1126/sciadv.aax8648

Inglis, E.C., Creech, J.B., Deng, Z., Moynier, F. (2018) High-precision zirconium stable isotope measurements of geological reference materials as measured by double-spike MC-ICPMS. *Chemical Geology* 493, 544–552. https://doi.org/10.1016/j.chemgeo.2018.07.007

Inglis, E.C., Moynier, F., Creech, J., Deng, Z., Day, J.M.D., Teng, F.-Z., Bizzarro, M., Jackson, M., Savage, P. (2019) Isotopic fractionation of zirconium during magmatic differentiation and the stable isotope composition of the silicate Earth. *Geochimica et Cosmochimica Acta* 250, 311–323. https://doi.org/10.1016/j.gca.2019.02.010

Harrison, T.M., Watson, E.B. (1983) Kinetics of zircon dissolution and zirconium diffusion in granitic melts of variable water content. *Contributions to Mineralogy and Petrology* 84, 66–72. https://doi.org/10.1007/BF01132331

Méheut, M., Ibañez-Mejia, M., Tissot, F.L.H. (2021) Drivers of zirconium isotope fractionation in Zr-bearing phases and melts: The roles of vibrational, nuclear field shift and diffusive effects. *Geochimica et Cosmochimica Acta* 292, 217–234. https://doi.org/10.1016/j.gca.2020.09.028

Melnik, O.E., Bindeman, I.N. (2018) Modeling of trace elemental zoning patterns in accessory minerals with emphasis on the origin of micron-scale oscillatory

zoning in zircon. *American Mineralogist* 103, 355–368. https://doi.org/10.2138/am-2018-6182

Tian, S., Moynier, F., Inglis, E.C., Rudnick, R.L., Huang, F., Chauvel, C., Creech, J.B., Gaschnig, R.M., Wang, Z., Guo, J.-L. (2021) Zirconium isotopic composition of the upper continental crust through time. *Earth and Planetary Science Letters* 572, 117086. https://doi.org/10.1016/j.epsl.2021.117086

Tissot, F.L.H., Ibañez-Mejia, M. (2021) Unlocking the Single-Crystal Record of Heavy Stable Isotopes. *Elements* 17, 389–394. https://doi.org/10.2138/gselements.17.6.389

Tompkins, H.G.D., Zieman, L.J., Ibañez-Mejia, M., Tissot, F.L.H. (2020) Zirconium stable isotope analysis of zircon by MC-ICP-MS: methods and application to evaluating intra-crystalline zonation in a zircon megacryst. *Journal of Analytical Atomic Spectrometry* 37, 1167–1186. https://doi.org/10.1039/C9JA00315K

Watkins, J.M., DePaolo, D.J., Watson, E.B. (2017) Kinetic Fractionation of Non-Traditional Stable Isotopes by Diffusion and Crystal Growth Reactions. *Reviews in Mineralogy and Geochemistry* 82, 85–125. https://doi.org/10.2138/rmg.2017.82.4

Zhang, W., Wang, Z., Moynier, F., Inglis, E., Tian, S., Li, M., Liu, Y., Hu, Z. (2019) Determination of Zr isotopic ratios in zircons using laser-ablation multiple-collector inductively coupled-plasma mass-spectrometry. *Journal of Analytical Atomic Spectrometry* 34, 1800–1809. https://doi.org/10.1039/C9JA00192A

Zhang, Y., Ni, H., Chen, Y. (2010) Diffusion Data in Silicate Melts. *Reviews in Mineralogy and Geochemistry* 72, 311–408. https://doi.org/10.2138/rmg.2010.72.8

The rises and falls of zirconium isotopes during zircon crystallisation

I.N. Bindeman, O.E. Melnik

Supplementary Information

The Supplementary Information includes:

- Mathematical Model
- MATLAB Code User Guide
- Supplementary Figures S-1 to S-4
- Supplementary References

Mathematical Model

Zircon growth in the center of a spherical melt cell (Fig. 1) proceeds from a diffusion of mixture of zirconium isotopes dissolved in their natural abundance proportion the silicate melt towards the growing crystal as is described by a diffusion equation with corresponding boundary conditions.

$$\frac{\partial C_i}{\partial t} = \frac{D_i(T, X_{H_2O})}{r^2}\left(\frac{\partial}{\partial r} r^2 \frac{\partial C_i}{\partial r}\right); i = Zr^{90,91,92,94,96}, Tr \qquad \text{(Eq. S-1)}$$

Here C_i is the concentration of a stable isotope of zirconium or a trace element, measured in ppm, r is the radius counted from the center of the zircon crystal, and t is time. Equation S-1 is solved only inside the melt part of the cell, $s < r < R$, because the diffusion of Zr and trace elements in the zircon crystal are negligibly slow (Cherniak and Watson, 2007) in comparison with their diffusion in the melt (Zhang *et al.*, 2010). Boundary conditions at the crystal-melt interface ($r = s$) postulate a local thermodynamic equilibrium, mass conservation of Zr isotopes and trace elements, and the partition of trace elements.

$$r = s: -\rho_m D_i \left.\frac{\partial C_i}{\partial r}\right|_{r=s} = J_i = V\left[\rho_m C_i^m - \rho_s C_i^s\right]; \sum_{i=1}^{5} C_{Zr^i}^m = C_{sat}(T), C_{Tr}^s = K(T) C_{Tr}^m. \qquad \text{(Eq. S-2a)}$$

Here ρ_s and ρ_m are the densities of zircon crystal and the melt, respectively, $C_{sat}(T)$ is the saturation concentration of zirconium in the melt in equilibrium with a zircon (per Watson and Harrison, 1983; Boehnke *et al.*, 2013). We assume that $C_{sat}(T)$ is the summed concentration of zirconium isotopes at their natural bundance. $K(T)$ values are the partition coefficients of trace elements of interest between the melt and the zircon crystal (Rubatto and Hermann, 2007). On the

outer melt boundary ($r = R$), mass partitioning of Zr isotopes and trace elements between major minerals and the melt is specified:

$$r = R : -D_i \left.\frac{\partial C_i}{\partial r}\right|_{r=R} = J_i = W\left[C_{m,i} - C_{X,i}\right];\ C_{X,i} = kC_{m,i}. \qquad \text{(Eq. S-2b)}$$

Here W is the velocity of the outer boundary controlled by changes in the melt fraction due to the crystallisation of major minerals, C_X is the concentration of zirconium and trace elements in these major minerals, and k is the distribution coefficient $C_{Zr}^{major}/C_{Zr}^{melt}$. As Zr and other trace elements considered here (Hf, U, Th, Y, P, Ti) are incompatible in major minerals, in most cases k is less than 0.1, but the value can be adjusted by the user for different minerals and assemblages of minerals. Crystallisation of major mineral on the outer boundary of the melt cell leads to enrichment of remaining melt with Zr (and trace elements; Figs. 2, S-3) leading to the local zircon oversaturation near the major mineral/melt boundary (*e.g.*, Bacon, 1989).

Sorokin *et al.* (2022) demonstrated that zircon crystallizing from typical rhyolitic magma cannot achieve greater than 30 ppm oversaturation without crystallising a microzircon. In such a situation, k of major mineral + microzircon is chosen to be close to 1. We therefore made a function within a program that can make k a function of oversaturation, that can be selected or deselected by the user.

The model is realized in MATLAB and optimized for computational efficiency using implicit method. Further details for the implementation of the model can be found in Bindeman and Melnik (2016) and Melnik and Bindeman (2018).

For validation of this model for zirconium isotopes, we checked their mass conservation in the entire cell (as in Fig. 1). The total mass of a zirconium isotopes is equal to the sum of their masses in zircon, melt, and major phases:

$$M_i = 4\pi\left(\int_0^s C_{Zr^i}^S r^2 dr + \int_s^R C_{Zr^i}^m r^2 dr + \int_R^{R_0} C_{Zr^i}^{major} r^2 dr\right) \qquad \text{(Eq. S-3)}$$

The error of zircon mass conservation remains within ±1 % of the initial Zr mass even for a coarse mesh and large timesteps (Fig. S-1a), corresponding to variations on the $\delta^{94/90}$Zr parameter <0.01 ‰. We further checked for the results for their independence on the radial computational mesh density (Fig. S-1b) and found that the zircon radius only slightly changes with a transition to finer meshes.

MATLAB Code User Guide

The MATLAB Code used herein is available from GitHub at https://github.com/crystalworkshop/isotop_diffusion. Users need not have experience with MATLAB programming to run the model to get results of simulations. The below instructions provide a key to parameters change.

Copy two folders (*functions* and *Results*) and one file (*main.m*) into the same folder. File *main.m* runs the program by using subroutines (functions) in the *functions* folder and results of the simulation appear in the *Results* folder as a text file and a series of graphs (see Fig. S-2). Use lines 14–24 in *main.m* to change input parameters: Zr concentration in the melt, water content (XH2O), size of the cell (length), and ratio of diffusion coefficients of other trace elements of interest to Zr in the melt. Lines 32 (Tend) and 33(tfin) set up the final temperature of crystallisation (in °C) and time in years. Cooling and crystallisation are set from T of zircon saturation as a linear T-t function along the phase diagram. Phase diagram (Temperature-% crystals) is set using Piwinski (1968) with a concave down function to account for eutectic crystallisation, a much smaller T change for the last 30 % of crystallization. Longer crystallisation durations may require increasing the number of time steps nt = 500 (line 14) to a greater number.

You can choose the trace element by name at line 41 (inside the *functions* folder, the function *kdHf.m* allows to use partition coefficients of trace elements taken from Melnik and Bindeman, 2018).

File *TemperatureHistory.m* controls the temperature-time history, which is linear in the present model; users can construct and insert their own, for example the heat propagation equations from Bindeman and Melnik (2016) for natural temperature-time histories in and around cooling intrusions. File *ZrSaturation.m* chooses the zircon saturation equation among published models: Watson and Harrison (1983) is used in the present model, but users can uncomment the Boehnke *et al.* (2013) line to use it instead. *DiffusionCoefficient.m* parameterises diffusion coefficients of Zr as a function of temperature and water content in the melt from Zhang *et al.* (2010).

Supplementary Figures

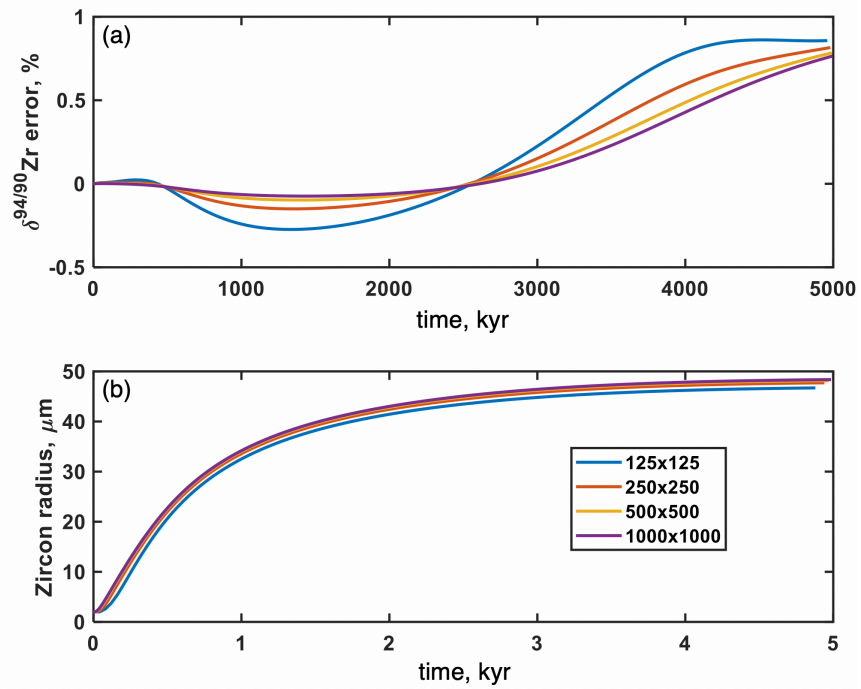

Figure S-1 Validation of the model using mass conservation of Zr isotopes in the cell (see Fig. 1) **(a)** during zircon crystallisation and **(b)** as a function of different mesh sizes.

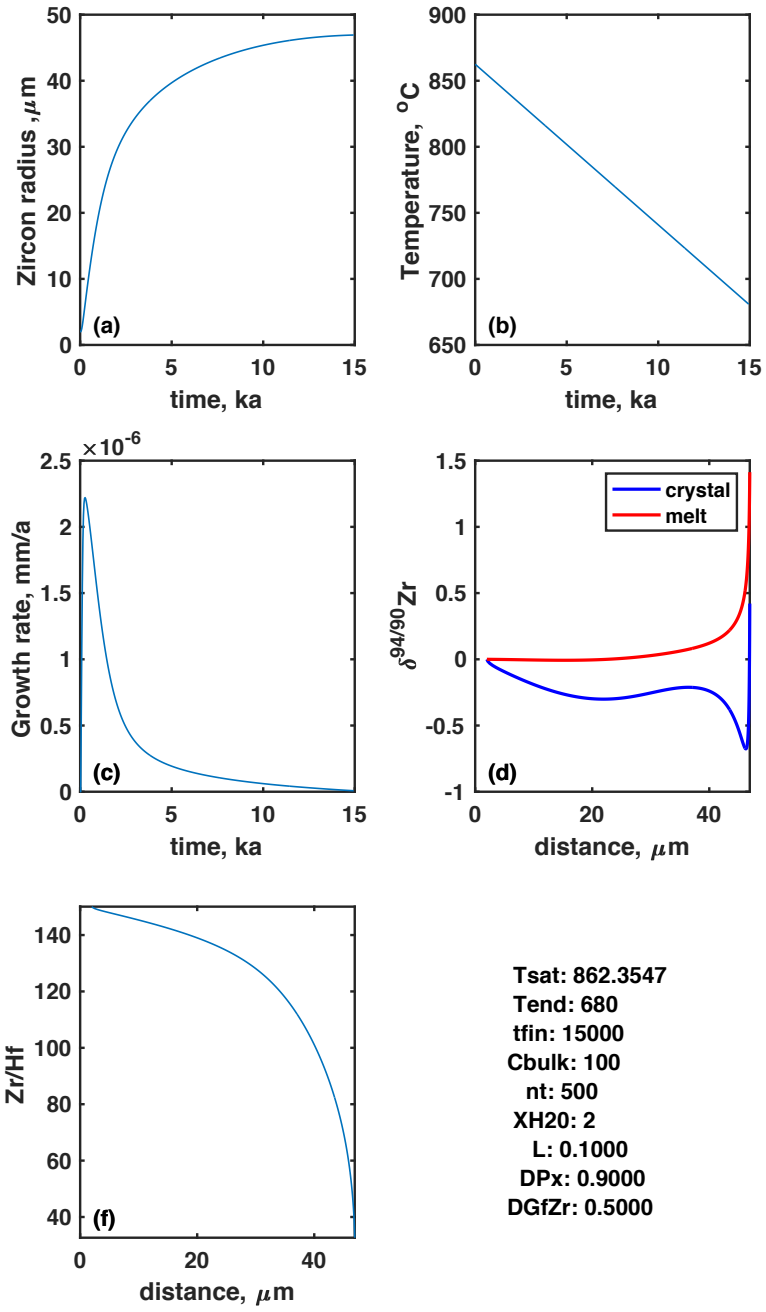

Figure S-2 Graphical output of the computation at given crystallisation conditions. The $\delta^{94/90}$Zr value in melt is the average value of the entire remaining melt volume in a cell at the moment of a particular zircon layer crystallisation.

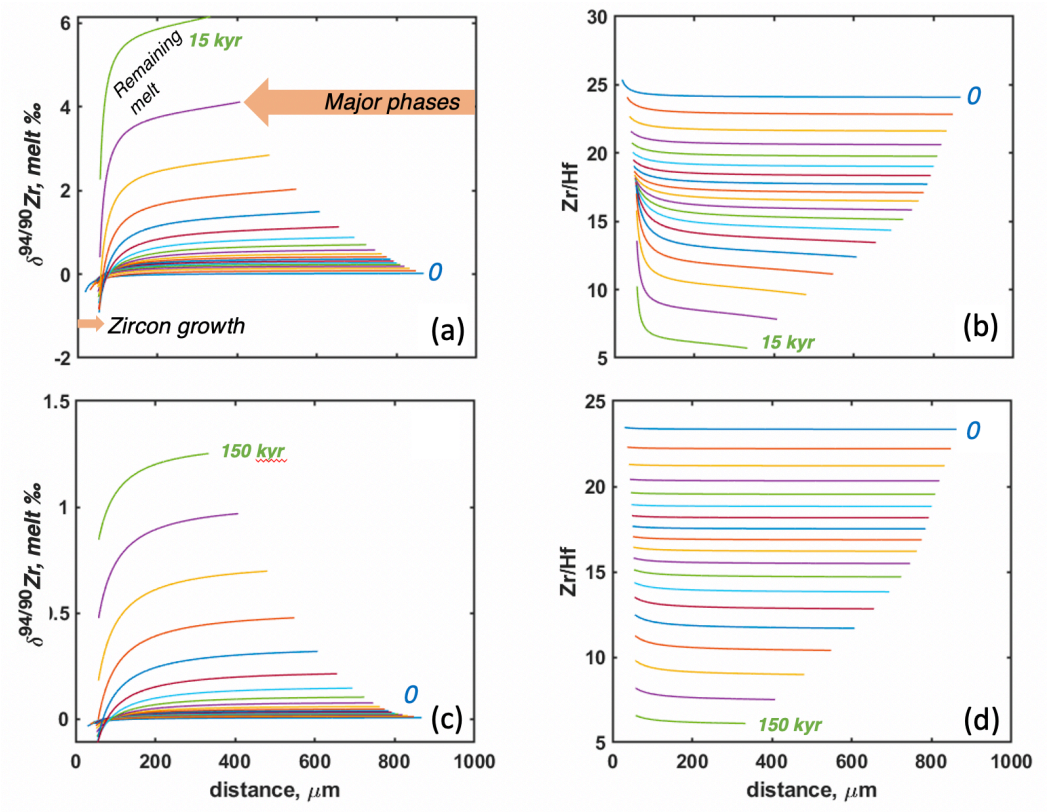

Figure S-3 Crystallisation of a melt cell as in Figure 1 from 950 °C to 680 °C (zircon saturation is at 862 °C) resulting in changes in the $\delta^{94/90}$Zr and Zr/Hf ratios. **(a, b)** rapid crystallisation over 15 kyr, 2 wt. % H_2O. **(c, d)** 150 kyr in a melt with 5 wt. % H_2O. Note smaller isotope and Zr/Hf effects. All graphs have Hf/Zr diffusion coefficient ratio = 0.4. Compare to Figure 2 in the main text for 1.5 kyr crystallisation duration.

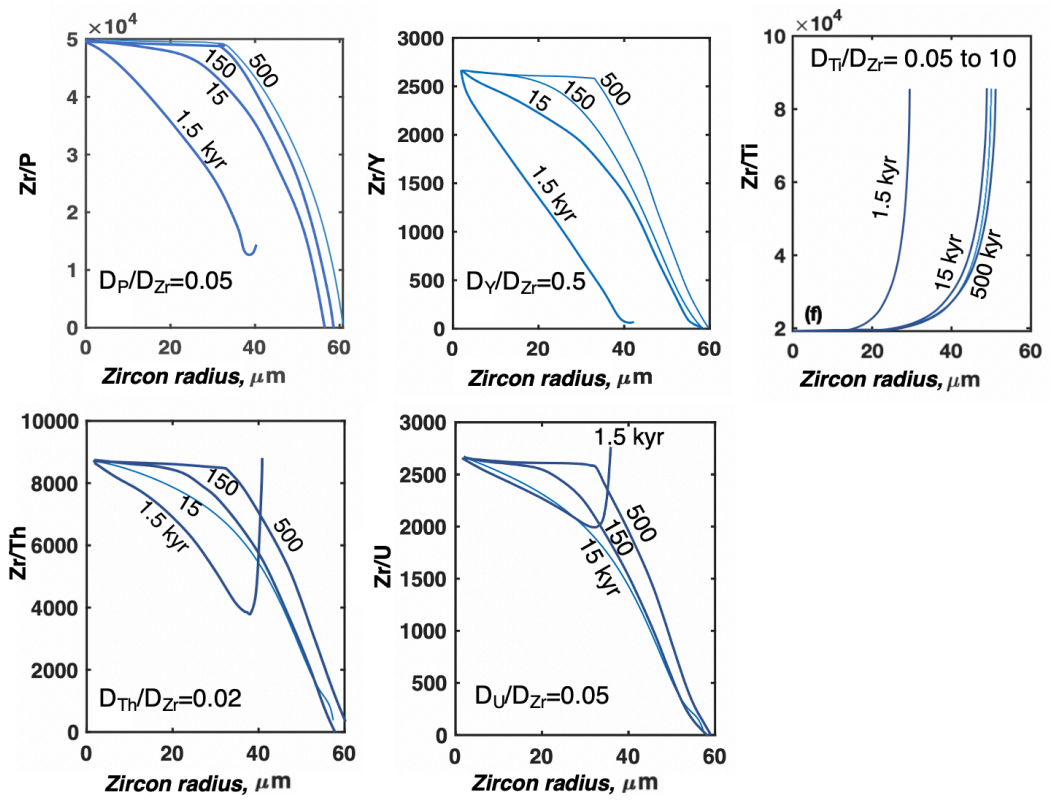

Figure S-4 Trace elemental profiles through zircon crystal at different crystallisation duration. See Figure 4 in the main text for Hf. Parameters are: 100 ppm Zr in the melt cell of 1 mm in radius, crystallising from 862 °C saturation to near solidus at 680 °C, H_2O_{melt} = 2 wt. %, Kd of Zr and other trace elements between major minerals and melt are 0.1. Note that shorter crystallisation durations result in steeper elemental profiles and inversions for these highly compatible elements as well as Hf (Fig. 4). Inversions are due to counterplay of piling up effects of compatible elements during rapid zircon growth in the zircon boundary layer, and an increase in K_d with decreasing temperature when diffusion slows down at low temperature. As zircon has a nearly constant 480,000 ppm Zr, trace elemental concentrations are a simple inverse of the ratio shown. Elements incompatible in zircon (such as Ti) do not exhibit kinetically induced enrichment near zircons, the increase in Zr/Ti ratio (decrease in Ti concentration) is only due to K_d^{Ti} increase with decreasing temperature and do pile up around major minerals. These diffusion and partition parameters are adopted from Melnik and Bindeman (2018; see their Fig. 3), and can be implemented in the present program within *kdHf.m* file (see instructions above).

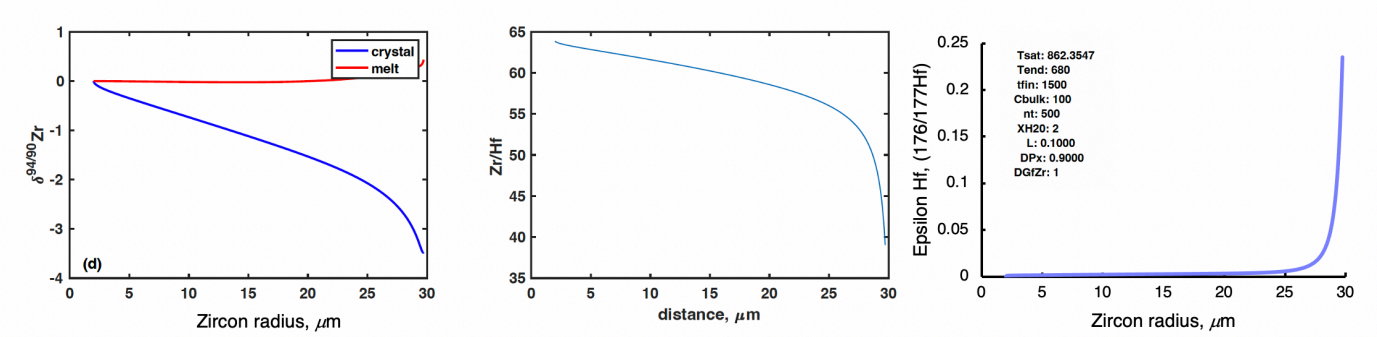

Figure S-5 Hf stable isotope fractionation within the model. ^{176}Hf and ^{177}Hf are assumed to have the same K_d between zircon and melt, but different diffusion coefficients, determined by the kinetic law: $D^{176}/D^{177} = (177/176)^{\beta}$, where $\beta = 0.05$ as for Zr isotopes. Because of the smaller mass difference between ^{176}Hf and ^{177}Hf and greater overall mass of Hf *vs*. Zr (masses 94 and 90), kinetic isotope fractionation is 0.03 ‰ in conditions shown, or 0.3 using epsilon units that are commonly used to describe Hf isotopes. Ratio of light to heavy isotopes for Hf (176/177) leads to the opposite trend than for Zr isotopes (94/90). Parameters are: 100 ppm Zr in the melt cell of 1 mm radius, crystallising from 862 °C saturation to near solidus at 680 °C, H_2O_{melt} = 2 wt. %, K_d of major phase is 0.9.

Supplementary Information References

Bacon, C.R. (1989) Crystallization of accessory phases in magmas by local saturation adjacent to phenocrysts. *Geochimica et Cosmochimica Acta* 53, 1055–1066. https://doi.org/10.1016/0016-7037(89)90210-X

Bindeman, I.N., Melnik, O.E. (2016) Zircon Survival, Rebirth and Recycling during Crustal Melting, Magma Crystallization, and Mixing Based on Numerical Modelling. *Journal of Petrology* 57, 437–460. https://doi.org/10.1093/petrology/egw013

Boehnke, P., Watson, E.B., Trail, D., Harrison, T.M., Schmitt, A.K. (2013) Zircon saturation re-revisited. *Chemical Geology* 351, 324–334. https://doi.org/10.1016/j.chemgeo.2013.05.028

Cherniak, D.J., Watson, E.B. (2007) Ti diffusion in zircon. *Chemical Geology* 242, 470–483. https://doi.org/10.1016/j.chemgeo.2007.05.005

Melnik, O.E., Bindeman, I.N. (2018) Modeling of trace elemental zoning patterns in accessory minerals with emphasis on the origin of micron-scale oscillatory zoning in zircon. *American Mineralogist* 103, 355–368. https://doi.org/10.2138/am-2018-6182

Piwinskii, A.J. (1968) Experimental studies of igneous rock series: Central Sierra Nevada Batholith, California. *The Journal of Geology* 76, 548–570. https://doi.org/10.1086/627359

Rubatto, D., Hermann, J. (2007) Experimental zircon/melt and zircon/garnet trace element partitioning and implications for the geochronology of crustal rocks. *Chemical Geology* 241, 38–61. https://doi.org/10.1016/j.chemgeo.2007.01.027

Sorokin, M.A., Melnik, O.E., Bindeman, I.N. (2022) Modeling of zircon nucleation and growth rates using crystal size distributions in a cooling magmatic intrusion. *Earth and Planetary Science Letters* 577, 117254. https://doi.org/10.1016/j.epsl.2021.117254

Watson, E.B., Harrison, T.M. (1983) Zircon saturation revisited: temperature and compositional effects in a variety of crustal magma types. *Earth and Planetary Science Letters* 64, 295–304. https://doi.org/10.1016/0012-821X(83)90211-X

Zhang, Y., Ni, H., Chen, Y. (2010) Diffusion Data in Silicate Melts. *Reviews in Mineralogy and Geochemistry* 72, 311–408. https://doi.org/10.2138/rmg.2010.72.8